Nonlinearity in a dynamo

P. Hejda[a]; M. Reshetnyak[b]

[a] Institute of Geophysics of the ASCR, 141 31 Prague, Czech Republic [b] Institute of the Physics of the Earth RAS, Moscow, Russia

First published on: 13 August 2010

PLEASE SCROLL DOWN FOR ARTICLE

Taylor & Francis
Taylor & Francis Group

Nonlinearity in a dynamo

P. HEJDA† and M. RESHETNYAK*‡

†Institute of Geophysics of the ASCR, Boční II/1401, 141 31 Prague, Czech Republic
‡Institute of the Physics of the Earth RAS, B. Gruzinskaya 10, Moscow, Russia

Using a rotating flat layer heated from below as an example, we consider effects which lead to stabilizing an exponentially growing magnetic field in magnetostrophic convection in transition from the kinematic dynamo to the full non-linear dynamo. We present estimates of the energy redistribution over the spectrum and helicity quenching by the magnetic field. We also study the alignment of the velocity and magnetic fields. These regimes are similar to those in planetary dynamo simulations.

Keywords: Boussinesq convection; Geostrophy; Quenching; Triads

1. Introduction

Many physical processes can be referred to threshold phenomena, when the increase of the governing parameter leads to the appearance of an increasing solution. Such an example is thermal convection, when the growth of thermal instability starts at a certain critical value of the Rayleigh number Ra^{cr}, which characterizes the amplitude of the heat sources (Chandrasekhar 1961). The same situation occurs if magnetic field $\mathbf{B}$ is generated in a conductive medium: the increase of the convection intensity, parameterized by the magnetic Reynolds number R_m, can lead to an exponentially growing solution (Moffatt 1978). After that magnetic field grows up to the moment when it starts to have an effect on the flow. As in many astrophysical objects R_m is very large, providing quite extended spectra of the fields, it is generally believed that this influence need not lead to a direct suppression of fluid motions. This statement is supported by the fact that in some cases transition from the non-magnetic to the magnetic state can be accompanied by the growth of Reynolds numbers. In other words, knowledge of R_m is not sufficient to answer the question whether the magnetic field will grow further or not.

The most widespread point of view is that the magnetic field causes such a reconstruction of the flow that the generation of the magnetic field becomes less efficient. However, the visual control of the flow does not reveal an essential change (Jones 2000), which can be due to the force-free nature of the magnetic

*Corresponding author. Email: m.reshetnyak@gmail.com

field configurations: $|(\nabla \times \mathbf{B}) \times \mathbf{B}|L_B/B^2 \ll 1$, where L_B is the energy-carrying scale of the magnetic field.

One of the explanations of the saturation mechanism is offered in Berger (1984) and Brandenburg and Subramanian (2005), where saturation is connected with the scale separation of the generated magnetic field due to conservation of magnetic helicity. In this article we study, on an example of the dynamo in a rapidly rotating flat layer heated from below, how such a magnetic energy redistribution over the spectra takes place in geostrophic systems. Our simulations demonstrate the occurrence of the magnetic α^M-effect which can suppress the total α-effect and lead to a saturated dynamo.

The other point is the correlation of velocity and magnetic fields (so-called cross helicity). It appears that a saturated velocity field can still lead to an exponentially growing magnetic field, provided that this new artificial magnetic field does not contribute to the Lorentz force. It was first noticed by Cattaneo and Tobias (2009), see also their KITP's conference video presentation. This problem has now become the subject of various discussions (Tilgner 2008, Tilgner and Brandenburg 2008, Schrinner *et al.* 2009). We also present some results concerned with the magnetostrophic regimes close to those in geodynamo simulations that are also unstable for large R_m.

2. Dynamo equations

The geodynamo equations for an incompressible fluid ($\nabla \cdot \mathbf{V} = 0$) in a layer of height L rotating with angular velocity Ω in a Cartesian system of coordinates (x, y, z) in its traditional geodynamo dimensionless form can be expressed as follows:

$$\frac{\partial \mathbf{B}}{\partial t} = \nabla \times (\mathbf{V} \times \mathbf{B}) + q^{-1}\Delta \mathbf{B},$$

$$EPr^{-1}\left[\frac{\partial \mathbf{V}}{\partial t} + (\mathbf{V} \cdot \nabla)\mathbf{V}\right] = -\nabla P - \mathbf{1_z} \times \mathbf{V} + RaTz\mathbf{1_z} + (\nabla \times \mathbf{B}) \times \mathbf{B} + E\Delta \mathbf{V}, \quad (1)$$

$$\frac{\partial T}{\partial t} + (\mathbf{V} \cdot \nabla)(T + T_0) = \Delta T.$$

The velocity $\mathbf{V}$, magnetic field $\mathbf{B}$, pressure P and the typical diffusion time t are measured in units of κ/L, $\sqrt{2\Omega\kappa\mu\rho}$, $\rho\kappa^2/L^2$ and L^2/κ, respectively, where κ is the thermal diffusivity, ρ is the density, μ the permeability, $Pr = \kappa/\nu$ is the Prandtl number, $E = \nu/(2\Omega L^2)$ is the Ekman number, ν is the kinematic viscosity, η is the magnetic diffusivity, and $q = \kappa/\eta$ is the Roberts number. $Ra = \alpha g_0 \delta T L/(2\Omega\kappa)$ is the modified Rayleigh number, α is the coefficient of volume expansion, δT is the unit of temperature, g_0 is the gravitational acceleration, and $T_0 = 1 - z$ is the heating from below. The problem is closed with periodic boundary conditions in the (x, y) plane. In the z-direction, we use simplified conditions (Cattaneo *et al.* 2003): for T and $\mathbf{V}$: $T = 0$ (heating from below), stress-free for $\mathbf{V}$: $V_z = \partial V_x/\partial z = \partial V_y/\partial z = 0$, and the pseudo-vacuum boundary condition for $\mathbf{B}$: $B_x = B_y = \partial B_z/\partial z = 0$ at $z = 0, 1$. System (1) was solved using the pseudo-spectral Fortran-95 MPI code (Reshetnyak and Hejda 2008) on cluster PC computers using grids N^3, $N = 64$.
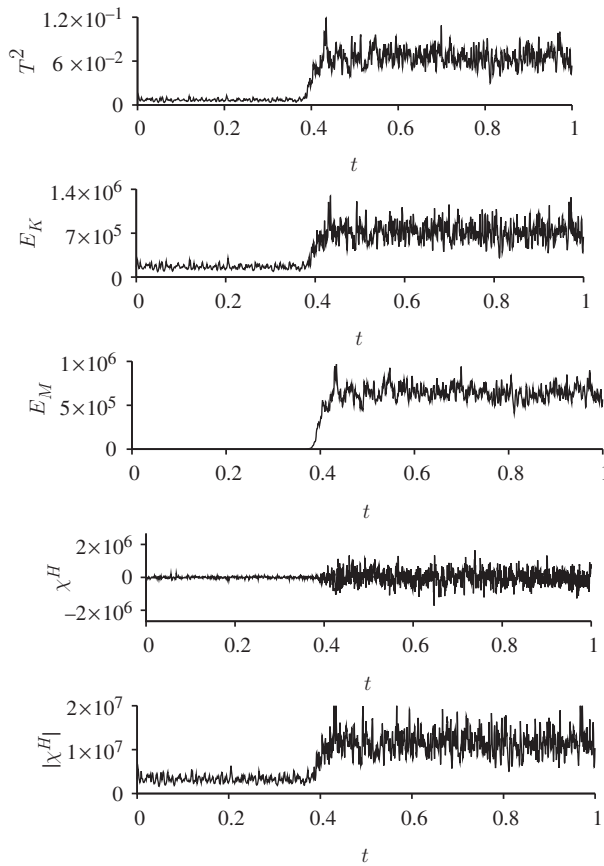
Figure 1. Regime R1. Evolution of the mean over the volume fluctuations of the squared temperature T^2, kinetic and magnetic energies E_K, E_M, and kinetic helicity χ^H, $|\chi^H|$.

3. Results of modelling

3.1. *General properties*

We consider two regimes that differ in Rayleigh and Roberts numbers:

R1: $Ra = 4 \times 10^2$, $Pr = 1$, $E = 2 \times 10^{-5}$, $q = 10$.
R2: $Ra = 1 \times 10^3$, $Pr = 1$, $E = 2 \times 10^{-5}$, $q = 3$.

To get the final saturated dynamo, we started from a pure convection state without the magnetic field. At time $t = 0.35$, we injected a magnetic field of small amplitude. After an intermediate kinematic regime with exponential growth of magnetic energy $E_M = \mathbf{B}^2/(2Ro)$, we arrive at a quasi-periodic state with kinetic, $E_K = \mathbf{V}^2/2$, and magnetic, E_M, energies of the same order of magnitude for R1 (figure 1), and at the state with $E_K > E_M$ for R2 (figure 2), where a smaller value of q was used.

Both regimes correspond to the geostrophic (magnetostrophic) state, see typical cyclonic structures of the temperature fluctuations T and kinetic energy E_K in figure 3 for R2. The diameter of the cyclones depends on the Ekman number as $d_c \sim LE^{1/3}$
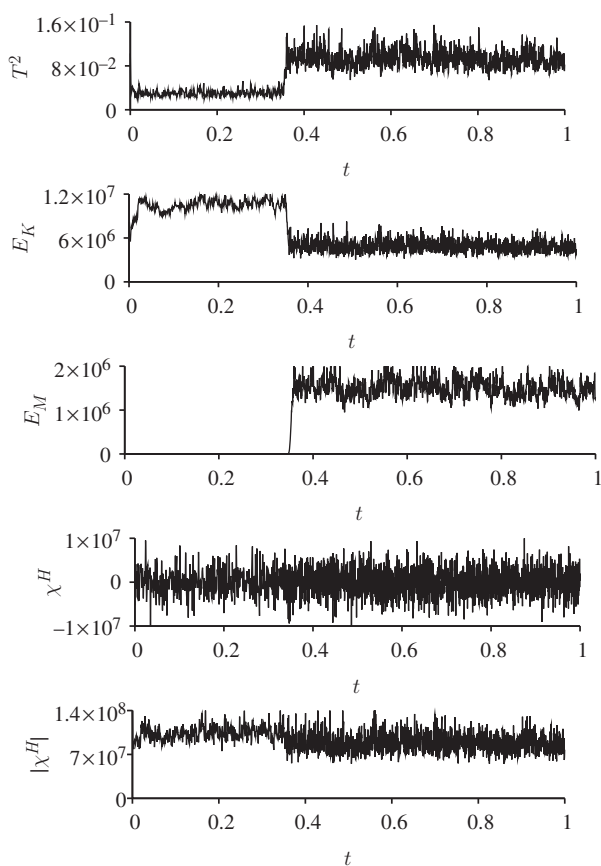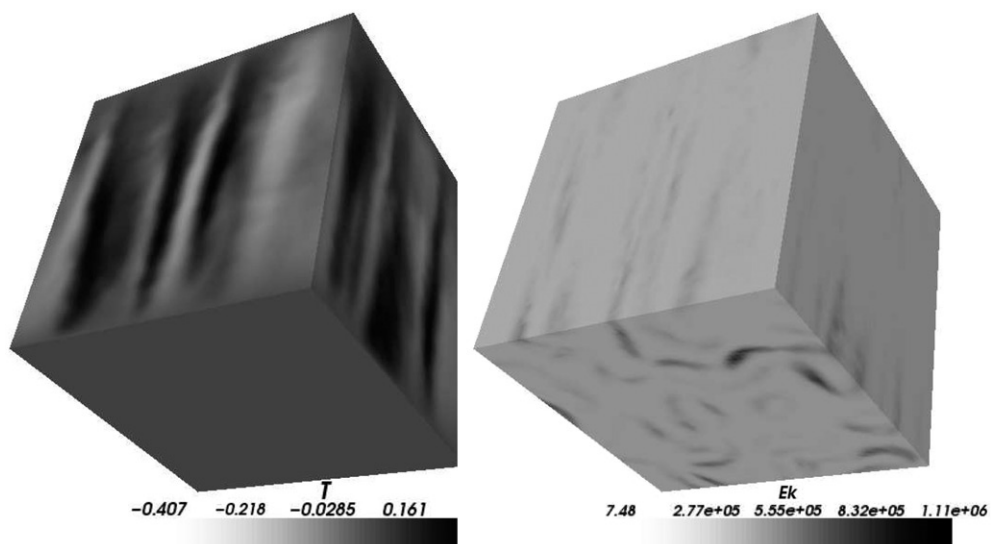
Figure 2.   The same as in figure 2 for regime R2.

Figure 3.   Distribution of temperature fluctuations T and kinetic energy E_K for regime R2.

(Busse 1970). In both cases the transition from the kinematic regime to the full dynamo was accompanied by an increase of the temperature fluctuations T^2.

On the other hand, the behaviour of the kinetic energy for the two regimes was different: for R1 the growth of the magnetic field leads to an increase in convection intensity (E_K becomes larger) and for R2 to a decrease. The corresponding Reynolds numbers are $Re = 200$ (kinematic dynamo regime) and $Re = 420$ (regime with saturation) for R1 and $Re = 1500$, 1100 for R2. For the observed geostrophic state the ratio of the nonlinear term in the Navier–Stokes equation to the Coriolis force, the Rossby number, $Ro = EV$ is quite small: $Ro = 4.3 \times 10^{-3}$, 8.4×10^{-3} for R1 and $Ro = 3.0 \times 10^{-2}$, 2.2×10^{-2} for R2. One of the explanations of the growth of Re for regime R1 is that the magnetic field disturbs the regular geostrophic flow for R1 and helps the generation of the magnetic field. The total energy $E_K + E_M$ also increases. Regime R2 corresponds to the more disturbed state, and the kinetic energy is reduced to the amount of increase of the magnetic energy. This scenario usually takes place for large Reynolds numbers. Note also that, while for R1 the increase of T^2 corresponds to the increase of the Archimedean work $RaTV_z$, for R2 the work decreases due to the chaotization of the fields. The behaviour of the kinetic helicity $\chi^H = \mathbf{V} \cdot \operatorname{curl} \mathbf{V}$ as a whole copies the evolution of the kinetic energy. The dispersion of χ^H increases when the magnetic field reaches its saturated value.

3.2. *Spectra*

The maximum of the kinetic energy spectra for R1 corresponds to the horizontal scale of the cyclones $k_c = 1/d_c$ (figure 4(a)). The magnetic field slightly decreases this maximum and kinetic energy increases. The relative part of the kinetic energy on the large scales also increases.

The growth of the magnetic field during transition from the kinematic dynamo state to saturation state is accompanied by an increase of the magnetic field on large scales (figure 4(b)). The first mode which reaches saturation is the mode with $k \sim 10$. The other modes still grow filling the spectra for E_M. This behaviour is the same for both the regimes R1, R2. The behaviour of the kinetic energy on the large scales is a little bit different for R2 (figure 4(c)), where we observe a decrease of E_K, which corresponds to the breakup of the horizontal rolls by the magnetic field. The maximum for E_K at $k = 1$ then disappears.

The inhomogeneous growth of the magnetic field for different k is quite important for understanding the saturation mechanism of the magnetic field. The growth of the magnetic field in the kinematic state takes place at convective times $\tau_k \sim (kV_k)^{-1}$, which decreases with k. According to Kazantsev (1968) the spectrum of the magnetic field is $E_M \sim k^{3/2}$ for the non-rotating turbulence, and the maximum of the magnetic field is then close to the dissipative scales. In our regime, the maximum of E_K at $k = k_c$ is more important for the magnetic field distribution, and the modes with $k \sim k_c$ reach saturation level at first. We argue that this regime is closely connected with the occurrence of the coherent structures discussed in Tobias and Cattaneo (2008).

The observed redistribution of the magnetic field over the scales is closely related to the mean over the volume magnetic helicity $\chi^{\mathcal{M}} = \mathbf{A} \cdot \mathbf{B}$ for $R_m \to \infty$ (Berger 1984),
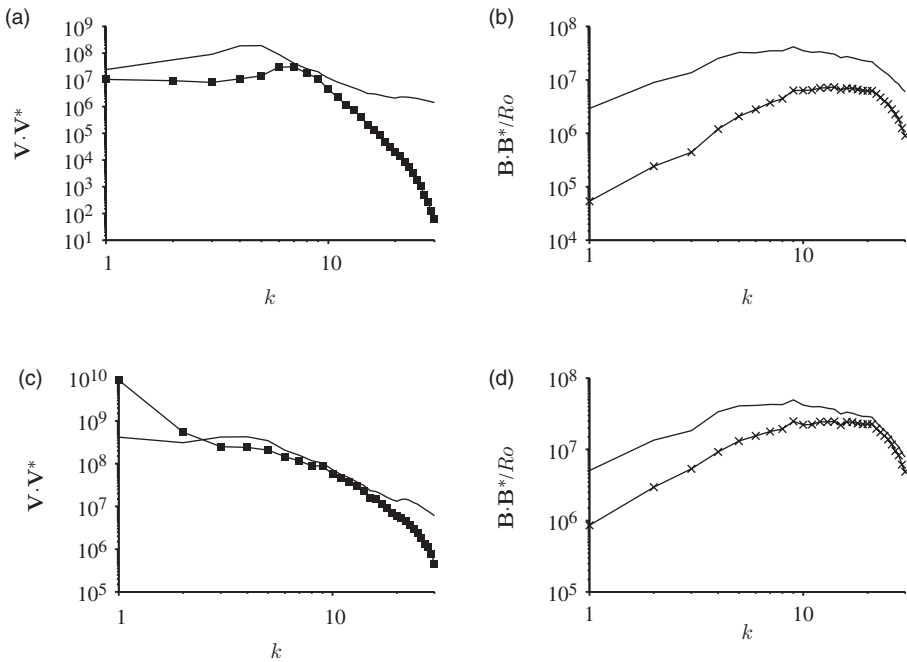
Figure 4. Spectra of the kinetic and magnetic energies for regime R1 (a–b) and R2 (c–d). The solid line correspond to the saturated dynamo, squares to the convection without magnetic field, and crosses to the kinematic dynamo regime.

where $\mathbf{A}$ is the vector potential of the magnetic field $\mathbf{B} = \mathrm{curl}\,\mathbf{A}^\dagger$. The alternating-sign quantity $\chi^{\mathcal{M}}$ is a measure of the linkage of the magnetic field lines with one another (Moffatt 1978). After some algebra with the induction equation, one arrives at the equation for the mean over the volume fields (Berger 1984, Brandenburg and Subramanian 2005)

$$\frac{\mathrm{D}}{\mathrm{D}t}\overline{\mathbf{A}\cdot\mathbf{B}} = -R_m^{-1}\overline{\mathbf{J}\cdot\mathbf{B}} + \Pi, \qquad (2)$$

where $\mathbf{J} = \mathrm{curl}\,\mathbf{B}$ is the current and Π is the flux of $\chi^{\mathcal{M}}$ through the boundary. $\Pi = 0$ for the fully periodic boundary conditions as well as for the super conductive boundaries. The other scalar product $\chi^{\mathcal{J}} = \mathbf{J}\cdot\mathbf{B}$ is the so-called current helicity.

Then, after time $t \sim R_m \gg 1$, one has saturation regime $\mathrm{D}/\mathrm{D}t = 0$, with

$$\overline{\mathbf{J}}\cdot\overline{\mathbf{B}} = -\overline{\mathbf{j}\cdot\mathbf{b}}, \quad \overline{\mathbf{A}}\cdot\overline{\mathbf{B}} = -\overline{\mathbf{a}\cdot\mathbf{b}}, \qquad (3)$$

where the decomposition of field F into the mean and fluctuating parts was used: $F = \overline{F} + f$ (Brandenburg and Subramanian 2005). In other words, after the kinematic regime no changes of the magnetic field would change the total magnetic and current helicities. Any local change is possible only due to the redistribution of $\chi^{\mathcal{M}}$, $\chi^{\mathcal{J}}$ over the scales. Of course, this approach becomes more complicated if the mean helicities change sign in space and the ideas on scale decomposition are applicable to the space domain with the same sign of helicity.

---

†Large R_m is typical for many astrophysical bodies which possess their own magnetic field.
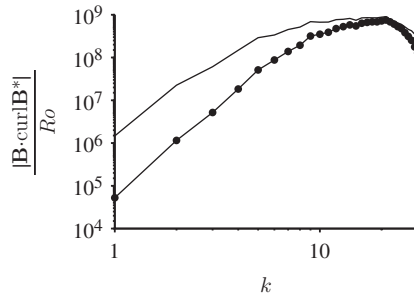
Figure 5. Spectra of the current helicity for regime R1. The solid line corresponds to the saturated dynamo, circles to the kinematic dynamo regime.

The application of the pseudo-vacuum boundary conditions, which provides $\Pi \neq 0$ at the boundaries, is more tricky. These conditions leads to the increase of the energy of the magnetic field at large scales (Brandenburg and Sandin 2004) and break the catastrophic quenching predicted by Vainshtein and Cattaneo (1992) and observed for the fully periodic boundary conditions (Hughes *et al.* 1996, Brandenburg and Subramanian 2005). There is also an indication of catastrophic quenching for the mean-field dynamo models with periodic boundary conditions (Cattaneo and Hughes 1996). According to this scenario the large-scale magnetic field B_0 would be saturated at $B_0^2 \sim R_m^{-1} b^2$, where $b^2 \sim v^2$ are the small-scale field energies.

In our simulations with pseudo-vacuum boundary conditions, we still observe some decrease of the magnetic field intensity (figures 1 and 2): the ratio of the magnetic to kinetic energies decreases from R1 to R2, which should be explained by a decrease of the Roberts number q rather than by catastrophic quenching. In figure 5 we also observe that the magnetic helicity on the large scales increases sufficiently after transition to the saturated regime.

Let us recall that, according to the mean field dynamo theory, there is connection between the kinetic and current helicities and hydrodynamic $\alpha^{\mathcal{H}}$- and magnetic $\alpha^{\mathcal{M}}$-effects for short correlation times (Pouquet *et al.* 1976, Zeldovich *et al.* 1983)

$$\alpha^{\mathcal{H}} = -\tau \overline{\mathbf{v} \cdot \boldsymbol{\omega}}/3, \quad \alpha^{\mathcal{M}} = \tau \overline{\mathbf{j} \cdot \mathbf{b}}/3, \tag{4}$$

where $\boldsymbol{\omega} = \text{curl}\, \mathbf{v}$ is the vorticity and τ is a correlation time. In practice (Zeldovich *et al.* 1983), these formulas are applicable when the typical time of the large-scale magnetic field growth τ_L is larger than the turnover kinetic time $\tau_t = l/v(l)$, where $v(l)$ is a velocity on scale l. A rough estimate of τ_L, using jump of the magnetic energy at the kinematic regime R1 (figure 1), yields $\tau_L \sim 10^{-2}$, which is already smaller than $\tau_t \sim 1/(Rek_c) \sim 10^{-3}$ (here we supposed that the kinetic energy is concentrated in the vicinity of k_c). Taking into account that the mean magnetic field grows slower than the small-scale field, we find that τ_L is even much larger than the above estimate (a similar situation for regime R2 takes place).

The total α-effect is then

$$\alpha = \alpha^{\mathcal{H}} + \alpha^{\mathcal{M}}. \tag{5}$$

If the signs of the helicities are the same, the total α-effect is reduced ($\alpha^{\mathcal{M}} \to -\alpha^{\mathcal{H}}$) and the magnetic field stops growing. The latter is well observed in our simulations,
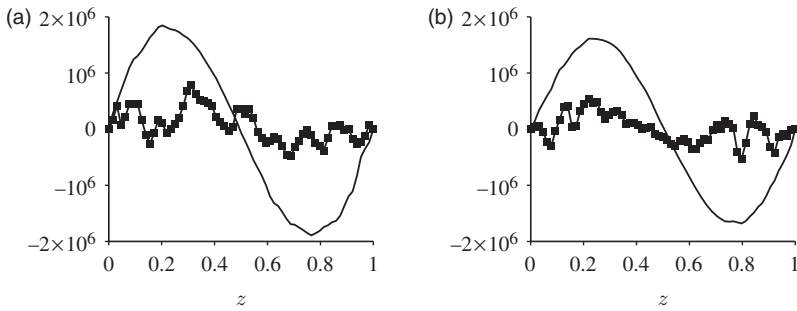
Figure 6. z-profiles of the kinetic χ^{H} (solid line) and current χ^{J} (squares) helicities for regimes R1 (a) and R2 (b).
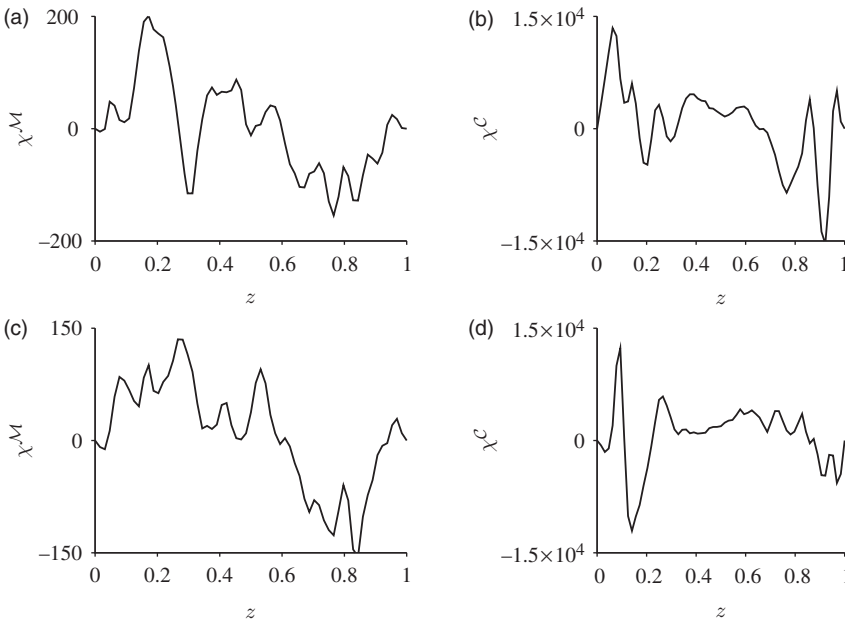

Figure 7. z-profiles of the magnetic χ^{M} and cross-χ helicities for regime R1 (a–b) and R2 (c–d).

figures 6 and 7, where $\chi^{CJM} > 0$ for $z < 0.5$ and $\chi^{CJM} < 0$ for $z > 0.5$. All the three helicities χ^{CJM} have the same signs, however, χ^{J} is more rugged due to the contribution of the small-scale fields.

3.3. *Energy fluxes in the wave space*

Energy redistribution over the spectra is closely related to the fluxes in wave space. In spite of the fact that the final saturated state is quasi-stationary, there are still fluxes in wave space. This happens because the scales where energy is generated and dissipated are different (Rose and Sulem 1978). For the simplest cases, such as 3D Kolmogorov's
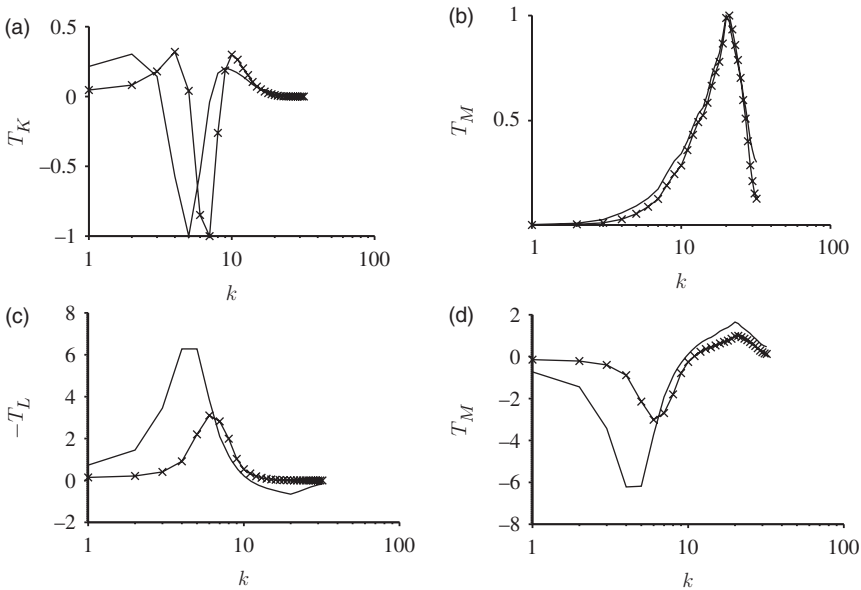
Figure 8. Fluxes in the wave space of the kinetic T_K and magnetic T_M energies, Lorentz work T_L and the convective term in the induction equation T_N, regime R1. The solid line corresponds to the saturated dynamo and crosses to the kinematic dynamo regime.

turbulence, kinetic energy goes from the scale of the force to the dissipative scale. Here we repeat the results of Reshetnyak and Hejda (2008) and Hejda and Reshetnyak (2009) and discuss the difference between energy fluxes of kinematic dynamo regime and the saturated regime.

Consider the kinetic energy flux in wave space through wave number k: $\mathcal{T}_K(k) = -\frac{\partial}{\partial k}$, where $\mathbf{V}^<(\mathbf{r}) = \sum_{|P| \le k} \widehat{\mathbf{V}}_P e^{i\mathbf{Pr}}$ is a low-frequency counterpart, and $\int_{k=0}^{\infty} \mathcal{T}_K(k)\, \mathrm{d}k = 0$.

Using relation curl $(\mathbf{V} \times \mathbf{B}) = -(\mathbf{V} \cdot \nabla)\,\mathbf{B} + (\mathbf{B} \cdot \nabla)\,\mathbf{V}$, the magnetic energy flux $\mathcal{T}_M(k)$ can be decomposed into advective and generating parts $\mathcal{T}_M = \mathcal{T}_N - \mathcal{T}_L$, $\int_{k=0}^{\infty} \mathcal{T}_N(k)\, \mathrm{d}k = 0$. The latter is equal to minus the work of the Lorentz force.

The fluxes of kinetic energy $\mathcal{T}_K$ are presented in figures 8(a) and 9(a). For $k \sim k_c$ the inverse cascade of kinetic energy is observed: the cyclones are the sources of the energy. Here energy is distributed to the large scales ($k < k_c$, $\mathcal{T}_K > 0$, inverse cascade), as well as to the small scales ($k > k_c$, $\mathcal{T}_K < 0$, direct cascade) where it dissipates. The magnetic field causes some blurring of the maxima and shift of $\mathcal{T}_K$ to the large-scale region.

In contrast to $\mathcal{T}_K$, $\mathcal{T}_M$ includes not only an advective term, but also a generating term. It appears that the integral of $\mathcal{T}_M$ over all k is positive. Moreover, $\mathcal{T}_M$ is positive for any k, figures 8(b), 9(b), i.e. the magnetic field is generated on small scales. Position of the maximum of $\mathcal{T}_M$ is close to the maximum in the spectrum of E_M. The form of $\mathcal{T}_M$ is the same for the small magnetic field during kinematic regime and for the saturated mode. Let us consider where the magnetic energy comes from: Is the energy transferred from other scales to some certain k, or is it generated localy? Generating flux $-\mathcal{T}_L$ is shown in figures 8(c) and 9(c). Its maximum is close to the minimum of $\mathcal{T}_K$ (R1), i.e. the kinetic energy is transformed to the energy of the magnetic field. Except for a small region at high k, there is always an inverse cascade of magnetic energy $-\mathcal{T}_L > 0$.
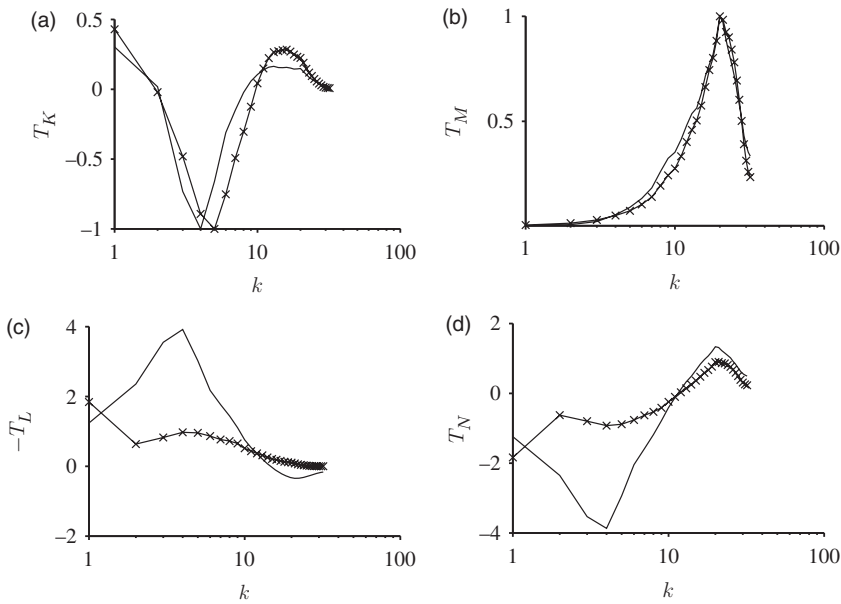
Figure 9. The same as in figure 8 for regime R2.

Note that the amplitudes of the maximum of $-\mathcal{T}_L$ and $\mathcal{T}_M$ are sufficiently different. That is because $-\mathcal{T}_L$ and $\mathcal{T}_N$ are anti-correlated (figures 8(d) and 9(d)). This means that advective term $\mathcal{T}_N < 0$ transports the major part of the energy to the dissipative scale.

Transition to the saturated state for R1 does not change the form of the flux's curve substantially. It only increases the amplitudes of $-\mathcal{T}_L$ and $\mathcal{T}_N$, thus increasing the synchronization of the fluxes $-\mathcal{T}_L$ and $\mathcal{T}_N$. The maxima of $-\mathcal{T}_L$ and $\mathcal{T}_N$ shift to the large scales for the full dynamo regime. For the R2-regime saturation changes the flux of the magnetic energy more efficiently. For the kinematic regime, the flux was more or less homogeneous from the small to large scales. For the saturated state, cyclones at k_c connected with decrease of E_M/E_K provide the main contribution to $-\mathcal{T}_L$. The relative strength of the total flux of the magnetic energy due to the $-\mathcal{T}_L$ term to the main scale remains at the same level. This flux can be related to the α-effect.

4. Alignment of the fields

In discussing z-profiles of the fields, we have not yet taken into account the importance of the spatial-temporal correlation of fields **V** and **B**. In this connection an interesting question arises: Can an already quenched velocity field in the dynamo model generate an exponentially growing magnetic field or not (Tilgner and Brandenburg 2008, Cattaneo and Tobias 2009)? The only one difference between this new passive magnetic field and the original one is that the new field does not contribute to the Lorentz force. It appears that the answer depends on the spectrum of the magnetic field and its time behaviour. Usually, if one has only one excited magnetic field mode for the saturated
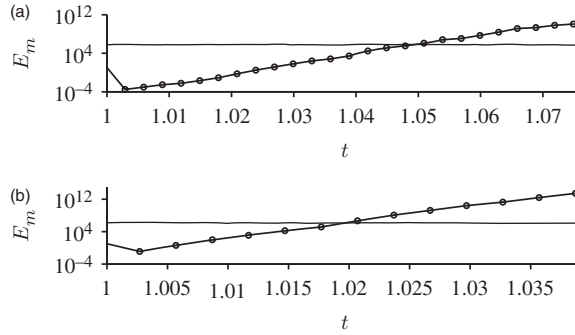
Figure 10. Evolution of the magnetic energies $\mathbf{B}^2/(2Ro)$ (solid line) and $\widehat{\mathbf{B}}^2/(2Ro)$ (circles) for regimes R1 (a) and R2 (b).

regime (Tilgner and Brandenburg 2008), the new passive magnetic field is stable. This statement is supported by simulations in the sphere (Tilgner 2008, Schrinner *et al.* 2009), where the dipole mode dominates for low Rossby number *Ro*. For the multi-mode regime (which is the case for the large Rayleigh number) the situation is different: the new magnetic field $\widehat{\mathbf{B}}$ grows exponentially (Cattaneo and Tobias 2009). There is an indication that the threshold for such a different behaviour of $\widehat{\mathbf{B}}$ in time in the sphere takes place at $Ro = 0.12$ (Schrinner *et al.* 2009). Here we consider what happens in the flat layer dynamo for regimes R1, R2 with quite extended spectra, adding a new induction equation for $\widehat{\mathbf{B}}$ to the system (1):

$$\frac{\partial \mathbf{B}}{\partial t} = \mathrm{curl}(\mathbf{V} \times \mathbf{B}) + q^{-1}\Delta\mathbf{B},$$

$$EPr^{-1}\left[\frac{\partial \mathbf{V}}{\partial t} + (\mathbf{V} \cdot \nabla)\mathbf{V}\right] = -\nabla P - \mathbf{1_z} \times \mathbf{V} + RaT z\mathbf{1_z} + (\nabla \times \mathbf{B}) \times \mathbf{B} + E\Delta\mathbf{V},$$

$$\frac{\partial T}{\partial t} + (\mathbf{V} \cdot \nabla)(T + T_0) = \Delta T, \tag{6}$$

$$\frac{\partial \widehat{\mathbf{B}}}{\partial t} = \mathrm{curl}\left(\mathbf{V} \times \widehat{\mathbf{B}}\right) + q^{-1}\Delta\widehat{\mathbf{B}}.$$

For both the regimes we observe distinct behaviours of B^2 and $\widehat{B}^2$ (figure 10). Although the same velocity field $\mathbf{V}$ was used in both the equations for $\mathbf{B}$ and $\widehat{\mathbf{B}}$, the new artificial magnetic field starts to grow exponentially. We are ready to conclude that temporal synchronization of the fields in space and time is crucial for stabilization. Field $\widehat{\mathbf{B}}$ is certainly less synchronized with velocity field $\mathbf{V}$ because the Lorentz force based on $\widehat{\mathbf{B}}$ has been omitted. This idea is supported by our simulations of the autocorrelation functions of the magnetic and velocity fields $\mathrm{Corr}(V_i, B_i)$, $\mathrm{Corr}(V_i, \widehat{B}_i)$ calculated over half of the volume $z \leq 0.5$ (figures 11 and 12). Evidently for both the regimes R1, R2 the correlation for $\widehat{\mathbf{B}}$ is less than for field $\mathbf{B}$. However, the correlation is quite small for both the regimes due to the stochastic nature of the small scale fields and does not exceed a few percent, reducing with increasing R_m. The reduction of correlation for all the components corresponds to the reduction of alignment of fields $\mathbf{V}$ and $\mathbf{B}$, when the Lorentz force is omitted. The real magnetic field $\mathbf{B}$ has stronger alignment. We adopt the explanation given by Cattaneo and Tobias (2009), Tilgner and
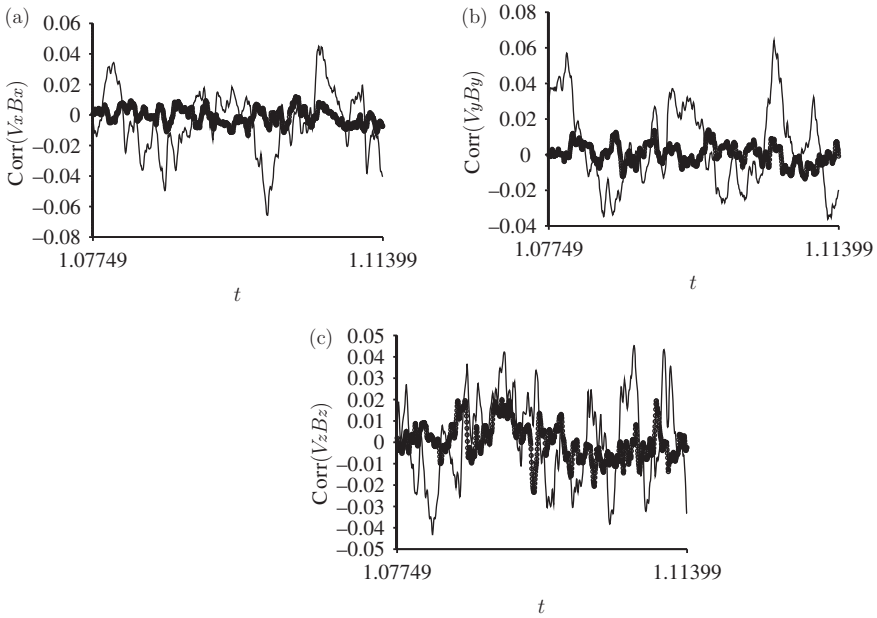
Figure 11. Evolution of the autocorrelation functions for regime R1. The thin line corresponds to the original magnetic field **B** and the line with circles to $\widehat{\textbf{B}}$.
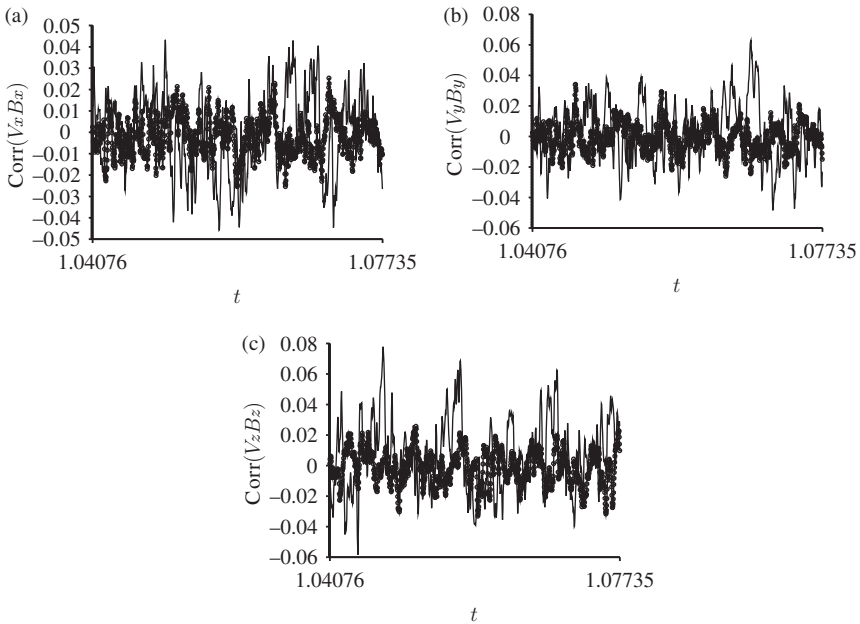

Figure 12. The same as in figure 11 for regime R2.

Brandenburg (2008) that the instability of $\widehat{\mathbf{B}}$ is due to the difference in the stability criteria for the full dynamo equation with quenched $\mathbf{V_q}$, and single induction equation with given $\mathbf{V_q}$.

5. Discussion

The transition from kinematic to saturated dynamo regime in cyclonic convection is accompanied by the reconstruction of the flow as well as of the magnetic field. In general, the change of the kinetic energy is not crucial: it can even increase during the transition. More important is the reconstruction of the flow patterns. The growing of the magnetic field $\mathbf{B}$ from the quasi-stationary convective state with non-zero kinetic helicity $\chi^H(z)$ is defined by the leading eigen solution. This first mode grows up to the level when the maximum of the spectra at $k \sim k_c$ reaches the saturated level close to the equipartition value on this scale. The growth of field $\mathbf{B}$ then stops at k_c. The small-scale field produces the magnetic $\alpha^{\mathcal{M}}$-effect which suppresses the total α-effect (5). According to (3), the transition to the saturated regime requires an increase of the large-scale magnetic field, which takes place at diffusion time $t \sim R_m$. Some change of the magnetic energy flux in the wave-space is also observed. The long-term fitting to the saturated regime is also predicted by the dynamical models of α-quenching (Kleeorin *et al*. 1995). During this time the large-scale magnetic field still grows to the limit defined by the restriction on the magnetic helicity conservation. The Lorentz force, which provides the correlation of the velocity and magnetic fields $\mathbf{V}$ and $\mathbf{B}$ and their alignment, plays a crucial role.

References

Berger, M.A., Rigorous new limits on magnetic helicity dissipation in the solar corona. *Geophys. Astrophys. Fluid Dynam*. 1984, **30**, 79–104.

Brandenburg, A. and Sandin, C., Catastrophic alpha quenching alleviated by helicity flux and shear. *Astron. Astrophys*. 2004, **427**, 13–21.

Brandenburg, A. and Subramanian, K., Astrophysical magnetic fields and nonlinear dynamo theory. *Phys. Rep*. 2005, **417**, 1–209.

Busse, F.H., Thermal instabilities in rapidly rotating systems. *J. Fluid Mech*. 1970, **44**, 441–460.

Cattaneo, F. and Hughes, D., Nonlinear saturation of the turbulent α-effect. *Phys. Rev*. 1996, **E 54**, R4532–R4535.

Cattaneo, F., Emonet, T. and Weiss, N., On the interaction between convection and magnetic fields. *Astrophp. J*. 2003, **588**, 1183–1198.

Cattaneo, F. and Tobias, S.M., Dynamo properties of the turbulent velocity field of a saturated dynamo. *J. Fluid Mech*. 2009, **621**, 205–214.

Chandrasekhar, S., *Hydrodynamic and Hydromagnetic Stability*, 1961 (Oxford, UK: Clarendon Press).

Hejda, P. and Reshetnyak, M., Effects of anisotropy in the geostrophic turbulence. *Phys. Earth Planet. Inter*. 2009, **177**, 152–160.

Hughes, D., Cattaneo, F. and Kim, E.J., Kinetic helicity, magnetic helicity and fast dynamo action. *Phys. Lett*. 1996, **A 223**, 167–172.

Jones, C.A., Convection-driven geodynamo models. *Phil. Trans. R. Soc. Lond*. 2000, **A 358**, 873–897.

Kazantsev, A.P., Enhancement of a magnetic field by a conducting fluid. *Sov. Phys. JETP* 1968, **26**, 1031–1039.

Kleeorin, N., Rogachevskii, I. and Ruzmaikin, A., Magnitude of the dynamo-generated magnetic field in solar-type convective zones. *Astron. Astrophys*. 1995, **297**, 159–167.

Moffatt, H.K., *Magnetic Field Generation in Electrically Conducting Fluids*, 1978 (Cambridge: Cambridge University Press).

Pouquet, A., Frisch, U. and Leorat, J., Strong MHD Helical Turbulence and the Nonlinear Dynamo Effect. *J. Fluid Mech*. 1976, **77**, 321–354.

Reshetnyak, M. and Hejda, P., Direct and inverse cascades in the geodynamo. *Nonlin. Proc. Geophys*. 2008, **15**, 873–880.

Rose, H.A. and Sulem, P.I., Fully developed turbulence and statistical mechanics. *J. Physique*. 1978, **39**, 441–484.

Schrinner, M., Schmidt, D., Cameron, R. and Hoyng, P., Saturation and time dependence of geodynamo models. *Geophys. J. Int*. 2010, **182**, 675–681.

Tilgner, A., Dynamo action with wave motion. *Phys. Rev. Lett*. 2008, **100**, 128501–128504.

Tilgner, A. and Brandenburg, A., A growing dynamo from a saturated Roberts flow dynamo. *Mon. Not. R. Astron. Soc*. 2008, **391**, 1477–1481.

Tobias, S.M. and Cattaneo, F., Dynamo action in complex flows: the quick and the fast. *J. Fluid Mech*. 2008, **601**, 101–122.

Vainshtein, S.I. and Cattaneo, F., Nonlinear restrictions on dynamo action. *Astrophys. J*. 1992, **393**, 165–171.

Zeldovich, Ya.B., Ruzmaikin, A.A. and Sokoloff, D.D., *Magnetic Fields in Astrophysics*, 1983 (NY: Gordon and Breach).